

The pairwise velocity dispersion of galaxies: luminosity dependence and a new test of galaxy formation models

Y.P. Jing^{1,2}, G. Börner^{2,1}

¹*Shanghai Astronomical Observatory, the Partner Group of MPI für Astrophysik,
Nandan Road 80, Shanghai 200030, China*

²*Max-Planck-Institut für Astrophysik, Karl-Schwarzschild-Strasse 1,
85748 Garching, Germany*

ABSTRACT

We present the first determination of the pairwise velocity dispersion (PVD) for galaxies in different luminosity intervals using the final release of the Two-Degree Field Galaxy Redshift Survey (2dFGRS). We have discovered quite surprisingly that the relative velocities of the faint galaxies at small separation are very high, around 700 km s^{-1} , reaching similar values as the brightest galaxies. At intermediate luminosities $M^* - 1$ (M^* is the characteristic luminosity of the Schechter function), the relative velocities exhibit a well defined steep minimum near 400 km s^{-1} . This result has been derived using a novel method to determine the real space power spectrum and the PVD from the redshift space power spectrum of the 2dFGRS. Combined with the observed luminosity dependence of clustering, our result implies that quite a fraction of faint galaxies, as well as the brightest ones, are in massive halos of galaxy cluster size, but most of the M^* galaxies are in galactic halos. Our observed result is compared with the current halo model of galaxies of Yang et al. that was obtained by matching the clustering and luminosity functions of the 2dFGRS. With the model parameters they favored most, the halo model seems to be unable to reproduce the luminosity dependence of the PVD because it predicts a monotonically increasing PVD with the luminosity. We discuss a possible solution to this model by raising the faint end slope of the conditional luminosity function in rich clusters. The PVD luminosity dependence may also be an important constraint in general on theories of galaxy formation, such as semi-analytical models and hydro/N-body simulations of galaxy formation.

Subject headings: galaxies: clustering - galaxies: distances and redshifts - large-scale structure of Universe - cosmology: theory - dark matter

1. Introduction

The clustering of galaxies in the Universe is characterized by their spatial positions, and by their peculiar velocities that lead to deviations of their motion from the pure Hubble flow. The big redshift surveys assembled in recent years by the diligent work of many astronomers give angular positions and redshifts for large numbers of galaxies. A rough 3D map can be obtained by placing the galaxies at distances along the line of sight derived via Hubble’s law from their redshifts. The peculiar velocity, however, also contributes to the redshift, and this leads to a misplacement of the galaxy away from its true location. The local gravitational field is the cause of the peculiar motion, thus the redshift distortion in the galaxy maps can give information on the underlying matter distribution.

The amplitude of the distortions can be estimated from the pair distribution of galaxies. For pairs of galaxies at distances much larger than their separation, one can use a plane-parallel approximation. In the linear approximation (or large separation), the power spectrum of their distribution in redshift space is (Kaiser 1987),

$$P^S(\mathbf{k}) = (1 + \beta\mu^2)^2 P(k). \quad (1)$$

Here μ is the cosine of the angle between the wave vector and the line of sight. The linear redshift distortion parameter β that is related to the linear growth factor $f(\Omega_0) \simeq \Omega_0^{0.6}$ (Ω_0 is the matter density) and the linear bias factor b of the galaxies by $\beta = \Omega_0^{0.6}/b$, can be estimated if $P^S(\mathbf{k})$ can be measured on a sufficiently large scale. $P(k)$ is the power spectrum in real space. The dependence on b expresses the fact that there is a bias in the galaxy distribution, i.e. there are differences between the galaxy and the dark matter distributions. The linear bias relation is just a constant ratio of the galaxy ξ and the dark matter ξ_{dm} two-point correlation functions (2PCF) $\xi = b^2 \xi_{dm}$. It has been shown that Eq.(1) is valid only on sufficiently large scales (perhaps $\gtrsim 20 h^{-1}\text{Mpc}$ or $k < 0.1 h\text{Mpc}^{-1}$, Scoccimarro 2004). On smaller scales, the virial motion of galaxies within groups and clusters contributes significantly to the deviation of the redshift distortion from the prediction of Eq.(1). In fact, on small scales ($\lesssim 5 h^{-1}\text{Mpc}$), the virial motion of galaxies dominates the redshift distortion.

Thus the redshift distortions on small scales can be used to determine the pairwise peculiar velocity dispersion (PVD) of galaxies. Assuming certain functional forms for the distribution function of the pairwise velocity (say, an exponential form, Peebles 1976) and for the average infall velocity, a model can be constructed for the redshift 2PCF which approximates the real situation well, when the coupling between the peculiar velocity and the spatial density of the galaxies is weak (Fisher et al. 1994b; Juszkiewicz, Fisher, & Szapudi 1998; Davis & Peebles 1983, hereafter DP83). A comparison of the model with observations of the redshift 2PCF provides a test for the validity of the assumptions (such as the distribution

function of the pairwise velocity) and a determination of the PVD $\sigma_{12}(r)$. DP83 applied this method to the CfA redshift survey, and determined the PVD to be $340 \pm 40 \text{ km s}^{-1}$ at projected separation $r_p = 1 h^{-1}\text{Mpc}$. Based on an extensive study of the PVD for all redshift surveys (typically containing 2000 galaxies) available before 1993, Mo, Jing, & Börner (1993) showed that the PVD measured is very sensitive to the presence of rich clusters in the survey. Because the CfA survey used by DP83 is too small to fairly represent the population of rich clusters in the Universe, Mo et al. pointed out that the PVD estimate given by DP83 is likely to be significantly biased low based on their analysis of the PVD for different surveys. Subsequent analyses for CfA2 by Marzke et al. (1995) and for CfA by Somerville, Davis, & Primack (1997) have confirmed the conclusion of Mo et al..

With the Las Campanas redshift survey (LCRS) of galaxies, Jing, Mo, & Börner (1998, hereafter JMB98) made the first accurate determination of the PVD using the above method. They used mock catalogs generated from N-body simulations of the concordance Λ cold dark matter (LCDM) model to correct for the observational effects including the fiber-collisions, and to make a fair estimation of errors for the measured PVD. They demonstrated that the errors of their measured PVD are between 50 and 100 km s^{-1} , and claimed that the PVD can be accurately measured with the LCRS, in contrast with all previous work based on smaller surveys. The PVD at the projected separation $1 h^{-1}\text{Mpc}$ is $570 \pm 80 \text{ km s}^{-1}$. This result has been verified by Zehavi et al. (2002) with the early data release of the Sloan Digital Sky Survey (SDSS). For IRAS galaxies, the PVD is lower than that of optical galaxies (Fisher et al. 1994a,b; Mo, Jing, & Börner 1993), and the PVD is very low on small scales (Jing, Börner, & Suto 2002; Hamilton & Tegmark 2002). These results of IRAS galaxies are also consistent with the SDSS study (Zehavi et al. 2002) where it was found that the PVD of the blue (young) galaxies is as low as that of IRAS galaxies. Cosmological hydrodynamic simulations of galaxy formation seem to lead to similar conclusions with regard to the PVD of different galaxy populations (Pearce et al. 2001; Yoshikawa, Jing, & Börner 2003; Berlind et al. 2003; Weinberg et al. 2004).

Another way to measure the PVD is to use the redshift space power spectrum. The redshift power spectrum $P^S(k, \mu)$ can be written as (Peacock & Dodds 1994; Cole, Fisher, & Weinberg 1995)

$$P^S(k, \mu) = P(k)(1 + \beta\mu^2)^2 D(k\mu\sigma_{12}(k)) \quad (2)$$

where the first term is the Kaiser linear compression, and the second term D is the damping effect caused by the random motion of the galaxies. For the exponential distribution function of the pairwise velocity, the function D is Lorentz form

$$D(k\mu\sigma_{12}(k)) = \frac{1}{1 + \frac{1}{2}k^2\mu^2\sigma_{12}(k)^2}. \quad (3)$$

Jing & Börner (2001a) have studied the redshift power spectrum in typical CDM models for different tracers –the primordial density peaks model, the cluster-underweighted scheme of particles, and pure dark matter, and found that different tracers may have different forms of the damping function. Thus, the damping function can serve as a constraint on galaxy formation models. From the analysis of the LCRS catalog, both Landy, Szalay, & Broadhurst (1998) and Jing & Börner (2001b) found that the damping function of observed galaxies is very close to Eq.(3). Adopting Eq.(3) for the damping function, Jing & Börner (2001b) measured the PVD $\sigma_{12}(k)$ for LCRS by setting $\beta = 0.45$ and found that the measured PVD is consistent with the PVD that JMB98 reported on the redshift 2PCF measurement. Hawkins et al. (2003) used Eq.(2) and Eq.(3) to model the redshift 2PCF with the Fourier transform, and measured the β and σ_{12} (assuming $\sigma_{12}(k) = \text{const.}$) for the Two-degree Field Galaxy Redshift Survey (2dFGRS) by best fitting the observed 2PCF. The advantage of using the redshift power spectrum to determine the PVD is that it is simple and accurate to model the infall effect.

Here we use the data of the final release of the 2dFGRS¹ for such an analysis to study the luminosity dependence of the PVD. The parameter β could, however, not be determined independently for each luminosity subsample, since there are still large statistical fluctuations on large scales $k\sigma\mu \leq 1$. Therefore, we fix β at a reasonable value of 0.45. Later we come back and consider the influence of a luminosity dependence (as in Norberg et al. 2002a) of β . Inspection of Fig. (9) shows that the results are basically unchanged, implying that the results are robust to reasonable changes of the β values.

The 2dFGRS has already been analysed statistically with respect to the PVD (Hawkins et al. 2003) and the determination of β (Peacock et al. 2001; Hawkins et al. 2003). But here we use a novel method to estimate the PVD. Furthermore, we take advantage of the large number of galaxies in the 2dFGRS to bin the galaxies in different luminosity intervals, and study the luminosity dependence of the PVD. This was not possible up to now, and we shall see that remarkable tests of galaxy formation models become possible with the statistical results presented here. The luminosity dependence of the clustering (the 2PCF) of galaxies in the 2dFGRS has been investigated (Norberg et al. 2001, 2002a,b) but not of the PVD.

It has been demonstrated already in an analysis of the LCRS (JMB98) that the observationally measured 2PCF and the PVD require a scale dependent bias model in order to find acceptable theoretical fits. The so-called cluster-underweighted model that was invented by JMB98 to bring a flat $\Omega = 0.2$ CDM model into agreement with the data has meanwhile been developed into a more sophisticated “halo-occupation-distribution” (HOD) model (e.g.

¹ Available at <http://www.mso.anu.edu.au/2dFGRS>

Sheth et al. 2001; Berlind & Weinberg 2002; Kang et al. 2002). In particular, Yang, Mo, & van den Bosch (2003, hereafter Y03) introduced the conditional luminosity function $\Phi(L|M)$ to characterize the luminosity distribution of galaxies within a halo of mass M , and measured the parametrized form of $\Phi(L|M)$ by matching the observed luminosity function of galaxies and the luminosity dependence of galaxy clustering in the 2dFGRS. This model has been applied to predict the clustering and velocity statistics of galaxies in the DEEP2 survey (Yan, Madgwick, & White 2003). By construction, the model of Y03 is able to reproduce the luminosity function and the two-point correlation function of galaxies. But the PVD, especially its luminosity dependence, can serve as an independent test on the model, as the PVD on small scales is rather sensitive to the HOD. We will show that the model most favored by Y03 is unable to match our measured luminosity dependence of the PVD, indicating that some of the parameterizations adopted by Y03 have to be amended. A comparison with the semi-analytic models for galaxy formation (Diaferio et al. 1999; Benson et al. 2000) will be presented in a subsequent investigation.

In the following chapters we describe our way of using the redshift power spectrum, the construction of mock catalogs from our simulations, tests of the method, the results, and the comparison with the HOD model of Y03. In the final discussion we summarize our results, and suggest construction principles for better models.

2. Observational sample and random sample

We select data for our analysis from the final release of the 2dFGRS (Colless et al. 2003, 2001, hereafter C01). The survey covers two declination strips, one in the Southern Galactic Pole (SGP) and another in the Northern Galactic Pole(NGP), and 99 random fields in the southern galactic cap. Each redshift determination is assigned a quality class Q in the 5-point system according to the measurement accuracy based on emission and absorption lines. Quality $Q = 1$ or 2 means a doubtful redshift estimate, $Q = 3$ means a probable redshift with the confidence 90 percent, and $Q = 4$ or 5 means a reliable redshift. Quality classes 1 and 2 are considered failures. The redshift sampling completeness $R(\theta)$ (θ is a sky position) that is defined as the fraction of targeted galaxies for which a redshift is measured with $Q \geq 3$, is available for each sky sector (C01). In this paper, only galaxies in the two strips are considered. Further criteria for galaxies to be included in our analysis are that they are within the redshift range of $0.02 < z < 0.25$, have the redshift measurement quality $Q \geq 3$, and are in the regions with the redshift sampling completeness $R(\theta)$ better than 0.1 (where θ is a sky position). The redshift range restriction should ensure that the clustering statistics are less affected by the galaxies in the local supercluster, and by the sparse sampling at

high redshift. The redshift quality restriction is imposed so that only galaxies with reliable redshift are used in our analysis. An additional reason is that the redshift completeness mask provided by the survey team, which is used in our analysis, is constructed for the redshift catalog of $Q \geq 3$. The last restriction is imposed in order to eliminate galaxies in the fields for which the field redshift completeness c_F is less than 70 percent (see C01 about the difference between $R(\theta)$ and c_F). These fields have not been included in computing the redshift mask map $R(\theta)$. As a result, there are a total of 190504 galaxies satisfying our selection criteria, 78190 in the NGP strip and 112314 in the SGP strip.

In order to study the luminosity dependence of the PVD, we divide the galaxies into 10 subsamples according to their absolute magnitude. The subsamples are successively brightened by 0.5 magnitude from the faintest sample $M_b = -17.0 + 5 \log_{10} h$ to $M_b = -21.5 + 5 \log_{10} h$, with successive subsamples overlapping by 0.5 magnitude. Here h is the Hubble constant in units of $100 \text{ km s}^{-1} \text{Mpc}^{-1}$. The details of the subsamples studied in this paper are given in Table 1. For computing the absolute magnitude, we have used the k-correction and luminosity evolution model of Norberg et al. (2002b, k + e model), i.e., the absolute magnitude is in the rest frame b_j band at $z = 0$. We assume a cosmological model with the density parameter $\Omega_0 = 0.3$ and the cosmological constant $\lambda_0 = 0.7$ throughout this paper.

A detailed account of the observational selection effects is released with the catalog by the survey team (C01). The limiting magnitude changes slightly across the survey region due to further magnitude calibrations that were carried out after the target galaxies had been selected for the redshift measurement. This observational effect is documented in the magnitude limit mask $b_J^{\text{lim}}(\theta)$ (C01). The redshift sampling is far from uniform within the survey region, and this selection effect is given by the redshift completeness mask $R(\theta)$. The redshift measurement success rate also depends on the brightness of galaxies, making fainter galaxies more incomplete in the redshift measurement. The $\mu(\theta)$ mask provided by the survey team is aimed to account for the brightness-dependent incompleteness. These effects can be corrected in computing the redshift two-point correlation function through constructing random samples that properly include these selection effects. We generate random samples in the same way as described in Jing & Börner (2004). Each random sample for a northern or southern luminosity subsample contains 100,000 random points.

3. Redshift power spectrum and the pairwise velocity dispersion

We measure the redshift two-point correlation functions $\xi_z(\mathbf{s})$ following the method of JMB98.

We convert the redshift two-point correlation function to the redshift power spectrum by the Fourier transformation:

$$P^S(\mathbf{k}) = \int \xi_z(\mathbf{s}) e^{-i\mathbf{k}\cdot\mathbf{s}} d\mathbf{s}. \quad (4)$$

In cylindrical polar coordinates (r_p, ϕ, π) with the π -axis parallel to the line-of-sight, $P^S(\mathbf{k})$ depends on k_p , the wavenumber perpendicular to the line-of-sight, and on k_π , the wavenumber parallel to the line-of-sight. The power spectrum can be written

$$P^S(k_p, k_\pi) = \int \xi_z(r_p, \pi) e^{-i[k_p r_p \cos(\phi) + \pi k_\pi]} r_p dr_p d\phi d\pi. \quad (5)$$

With some elementary mathematical manipulation, we get the following expression:

$$P^S(k_p, k_\pi) = 2\pi \int_{-\infty}^{\infty} d\pi \int_0^{\infty} r_p dr_p \xi_z(r_p, \pi) \cos(k_\pi \pi) J_0(k_p r_p) \quad (6)$$

where $J_0(k_p r_p)$ is the zeroth-order Bessel function (Jing & Börner 2001b).

$\xi_z(r_p, \pi)$ is measured in equal logarithmic bins of r_p and in equal linear bins of π . The reason why different types of bins are chosen for r_p and π is the fact that $\xi_z(r_p, \pi)$ decreases rapidly with r_p but is flat with π on small scales. Thus this way of presenting $\xi_z(r_p, \pi)$ is better than using the log-log or the linear-linear bins for r_p and π , and is also suitable for the present work. The peculiar velocity of a few hundred km s^{-1} should smoothen out structures on a few $h^{-1}\text{Mpc}$ in the radial direction, and the linear bin of $\Delta\pi_i = 1 h^{-1}\text{Mpc}$ is suitable for resolving the structures in the radial direction. With logarithmic bins chosen for r_p , the r_p dependence is resolved well, because otherwise the small scale clustering on the projected direction cannot be recovered. With this bin method, we obtain the power spectrum:

$$P^S(k_p, k_\pi) = 2\pi \sum_{i,j} \Delta\pi_i r_{p,j}^2 \Delta \ln r_{p,j} \xi_z(r_{p,j}, \pi_i) \cos(k_\pi \pi_i) J_0(k_p r_{p,j}) \quad (7)$$

where π_i runs from -50 to $50 h^{-1}\text{Mpc}$ with $\Delta\pi_i = 1 h^{-1}\text{Mpc}$ and $r_{p,j}$ from 0.1 to $50 h^{-1}\text{Mpc}$ with $\Delta \ln r_{p,j} = 0.23$ (Be careful not to confuse two π s in Eqs. (6) and (7): the first π in the right-hand-side has the conventional meaning, i.e. $3.14159\dots$, and the others are for the axis along the line-of-sight.). We make the summation of Eq.(7) with rectangular boundaries in π and r_p .

The fluctuations of $\xi_z(r_p, \pi)$ at large separations may bring errors to the determination of the redshift power spectrum. We improve the measurement by down weighting $\xi_z(r_p, \pi)$ at the larger scales. Specifically, we use a Gaussian window function

$$W_g(\mathbf{s}) = \exp\left(-\frac{1}{2} \frac{s^2}{S^2}\right) \quad (8)$$

to weight the two-point correlation function with $S = 20 h^{-1}\text{Mpc}$. That is, the measured redshift power spectrum is

$$P^{S,m}(k_p, k_\pi) = 2\pi \sum_{i,j} \Delta\pi_i r_{p,j}^2 \Delta \ln r_{p,j} \xi_z(r_{p,j}, \pi_i) W_g(r_{p,j}, \pi_i) \cos(k_\pi \pi_i) J_0(k_p r_{p,j}). \quad (9)$$

The weighting reduces the noise in the measurement, but introduces a systematic bias to the redshift power spectrum. This is the reason why we distinguish this measured redshift power spectrum $P^{S,m}(k_p, k_\pi)$ from the expression $P^S(k_p, k_\pi)$ in Eq.(7). But they are related by the following equation,

$$P^{S,m}(\mathbf{k}) = \frac{1}{(2\pi)^3} \int P^S(\mathbf{k}_1) W_g(\mathbf{k} - \mathbf{k}_1; S) d\mathbf{k}_1 \quad (10)$$

and

$$W_g(\mathbf{k}; S) = \frac{1}{(2\pi)^{3/2} S^3} \exp\left(-\frac{1}{2} S^2 k^2\right). \quad (11)$$

The weighting may change the redshift power spectrum at $k \lesssim \pi/S = 0.15 h\text{Mpc}^{-1}$, making the spectrum more isotropic and biasing the value of $P^S(k_p, k_\pi)$ generally. This effect can be estimated as follows. We take Eqs.(2) and (3) for the redshift power spectrum $P^S(\mathbf{k})$. As a typical example, we take $\beta = 0.45$, $\sigma_v = 500 \text{ km s}^{-1}$, and a linear Cold Dark Matter power spectrum from Bardeen et al. (1986) with the shape parameter $\Gamma = 0.2$ for $P^S(\mathbf{k})$, and compute $P^{S,m}(\mathbf{k})$ with Eq.(10). The result is plotted in Fig. (1) which is also compared with $P^S(\mathbf{k})$. The weighting makes the redshift power spectrum significantly rounder at $k = 0.1 h\text{Mpc}^{-1}$, but the effect becomes negligible for $k \gtrsim 0.2 h\text{Mpc}^{-1}$. Furthermore, the figure shows that the $P^S(k, \mu = 0)$ at $\mu = 0$ is changed little even at $k = 0.1 h\text{Mpc}^{-1}$, indicating that the real space power spectrum may be measured unbiasedly for $k \geq 0.1 h\text{Mpc}^{-1}$ (because $P(k) = P^S(k, \mu = 0)$).

A further test of the method is carried out by comparing the redshift power spectrum of a simulated galaxy catalog. The galaxy catalog is generated using the halo model (Y03, Yang et al. 2004, hereafter Y04) for a LCDM simulation of boxsize $300 h^{-1}\text{Mpc}$. The details about the CDM model, the simulation, and the method of generating the galaxies will be given in the next section. For our test, we select galaxies with luminosity in $-19.5 \leq M_b - \log_{10} h < -18.5$. We computed the redshift two-point correlation function by counting the galaxy pairs, and measure the redshift power spectrum using the procedure outlined above. These spectra are compared with the redshift power spectra measured with the Fourier transformation (FT) of the galaxy density field. This is shown in Fig. (2), with the symbols for $P(k, \mu)$ obtained with FT, and the line for those measured through the 2PCF. The power spectra measured with FT are free of the weighting effect [Eq.(10)]. The figure

confirms the results of Fig. (1), and indicates that our method can give an unbiased estimate of $P(k, \mu)$ for $k \geq 0.2 h\text{Mpc}^{-1}$ from which we will measure the velocity dispersion $\sigma_v(k)$ through equation (2). The real space power spectrum $P(k)$, which is mainly determined from $P^S(k, \mu = 0)$, can be determined for $k \geq 0.1 h\text{Mpc}^{-1}$.

4. Simulation, Halo model, and mock catalogs

We simulate galaxy catalogs using our cosmological N-body simulations. The cosmological model considered is a currently popular flat low-density model with the density parameter $\Omega_0 = 0.3$ and the cosmological constant $\lambda_0 = 0.7$ (LCDM). The shape parameter $\Gamma = \Omega_0 h$ and the amplitude σ_8 of the linear density power spectrum are 0.2 and 0.9 respectively. Two sets of simulations, with boxesizes $L = 100 h^{-1}\text{Mpc}$ and $L = 300 h^{-1}\text{Mpc}$, that were generated with our vectorized-parallel P³M code (Jing & Suto 2002; Jing 2002), are used in this paper. Both simulations use 512^3 particles, so the particle mass m_p is $6.2 \times 10^8 h^{-1} M_\odot$ and $1.7 \times 10^{10} h^{-1} M_\odot$ respectively in these two cases. We have four independent realizations for each boxsize. Dark matter halos are identified with the friends-of-friends method (FOF) using a linking length b equal to 0.2 times of the mean particle separation. All halos with ten members or more are included for generating the galaxy catalog.

We populate the halos with galaxies according to the prescription proposed by Y03. The luminosity function of galaxies in a halo is assumed to be a function of the halo mass M , $\Phi(L|M)$ that is further parametrized as the Schechter function. The parameters of the Schechter function are functions of M , further parametrized through the mass-to-light ratios of halos. There are a total of 8 parameters (without classifying galaxies with spectral types) that are determined by best fitting the observed luminosity function and the luminosity dependent clustering of galaxies in the 2dFGRS. It is shown by Yang et al. that these two observations are well reproduced by their model, but there is some degeneracy in the model parameters. In our work, we adopt model M1 in Y03 for the parameters of the halo model, and populate the halos with galaxies (the luminosity, position and velocity) in a similar way as Y04. The code for populating the halos with galaxies was, however, written by us independently. We adopt the “FOF satellites” scheme of Y04. We assign the satellite galaxies of a halo the position and velocity of dark matter particles randomly selected from the halo. Instead of locating the central galaxy at the center-of-mass of a halo as in Y04, we locate it at the potential minimum of the halo and assign its velocity with the halo bulk velocity. The mass resolution of the simulations sets a faint limit for which galaxies can be presented. According to Y04, galaxies are complete in the $300 h^{-1}\text{Mpc}$ simulation for magnitude brighter than $M_b - 5 \log_{10} h = -18.0$ and in the $100 h^{-1}\text{Mpc}$ simulation for

magnitude brighter than $M_b - 5 \log_{10} h = -15.0$. In Fig. (3), we present the luminosity functions of the model galaxies which do agree well with the observation of the 2dFGRS, and also agree with each other between the two sets of simulations.

It is straightforward to produce mock catalogs of the 2dFGRS, since we have the information of positions, velocity and luminosity for each galaxy. We first duplicate the simulation volumes periodically along the main axes, and execute the selection effects according to the observational masks. We produce 5 mock galaxy catalogs for each realization of a simulation, so we have a total 40 mock samples. For studying the redshift power spectrum of galaxies fainter than $M_b - 5 \log_{10} h = -18.0$, we will use the mock samples of the $100 h^{-1}\text{Mpc}$ simulations, otherwise we will use those of the $300 h^{-1}\text{Mpc}$ simulations.

It is important to understand the numerical artifacts of the simulations that may affect the result here. We believe that the force resolution of the simulations that adopt P^3M , are sufficient for the current study, since only the global information of halos is needed. The mass resolution has already been discussed above. It can be easily taken into account in our analysis. The boxsize may be the only concern that we need to consider seriously, because the most massive halos may be under-represented for the lack of long-wavelength density fluctuations, and the redshift power spectrum cannot be measured around the fundamental wavelength of the simulation. Since we measure $P(k, \mu)$ for $k \geq 0.1 h\text{Mpc}^{-1}$, we believe that the boxsize $300 h^{-1}\text{Mpc}$ is sufficiently large both for studying the large-scale clustering and for fairly sampling the massive clusters. To quantify the possible effect of the $100 h^{-1}\text{Mpc}$ boxsize, we measure the redshift power spectrum for the luminosity $-19.0 < M_b - 5 \log_{10} h < -18.5$ from the mock catalogs. The results of the two sets of mock catalogs are compared in Fig. (4), which clearly show that the simulation of $100 h^{-1}\text{Mpc}$ box size is sufficiently big in volume for studying the redshift power spectrum for $k > 0.16 h\text{Mpc}^{-1}$. Also the population of the halos that host the faint galaxies in the simulation of $100 h^{-1}\text{Mpc}$ should not be affected by the limited volume.

5. Results

The statistical quantities are defined in the Fourier space (\mathbf{k}) in the present work, which are often compared those obtained in the coordinate space (\mathbf{r}) in previous work. When doing this comparison, one uncertainty is the scale correspondence between the \mathbf{k} and \mathbf{r} spaces. Although the correspondence is $r = 2\pi/k$ in mathematics, we think that it is more appropriate to compare the two-point clustering and the PVD with the relation $r \Leftrightarrow 1/k$ based on the following facts. The two-point clustering can be expressed as a sum of two-halo and one-halo contributions (e.g. Kang et al. 2002). The transition from the two-halo

term dominance at large scales to the one-halo term dominance happens at $\sim 0.5 h\text{Mpc}^{-1}$ in k -space or at $r \sim 2 h^{-1}\text{Mpc}$ in the r -space for the concordance LCDM model (e.g. Kang et al. 2002, Y04). When comparing the scale dependence of PVD, Jing & Börner (2001a) also argued for $k \Leftrightarrow 1/r$. Therefore, we adopt $r \Leftrightarrow 1/k$ in the current paper when comparing the statistical quantities in the two spaces.

5.1. The luminosity dependence of the PVD

Our main results are shown in Figs. (5) to (8). In the introduction we have said that it should be possible to derive β , σ_{12} , and $P(k)$ from a measurement of the redshift space power spectrum $P^S(k, \mu)$. However, because we measure $P^S(k, \mu)$ only up to the scale $k = 0.1 h\text{Mpc}^{-1}$, there exists a strong degeneracy in determining the parameters σ_{12} and β (Peacock et al. 2001) from $P^S(k, \mu)$. Moreover, σ_{12} could be a function of k (Jing & Börner 2001a). We therefore fix $\beta = 0.45$ as a reasonable estimate (Hawkins et al. 2003), and then determine $P(k)$ and σ_{12} from the data. There could also be some luminosity dependence in β , and we investigate this by using the luminosity dependence of the bias parameter $b/b^* = 0.8 + 0.2(L/L^*)$ given in Norberg et al. (2002a) and $\beta^* = 0.45$, where the quantities with superscript $*$ are those at the characteristic luminosity M^* . The result is shown in Fig. (9). The PVD for the brightest galaxies is slightly increased compared to the result in Fig. (8), and it is slightly decreased for the faint galaxies. The changes are small, therefore it seems justified to use a constant β . In Figs. (8) and (9) we have also plotted the PVD values at the number-weighted luminosity value in each bin.

In Fig. (5) the basic measurement of the power spectrum in redshift space $P^S(k, \mu)$ is shown. The four panels in this figure correspond to four different luminosity intervals (samples 3, 5, 7, and 9 of table 1) from faint to bright galaxies. The symbols are the results for the full 2dFGRS, the dotted lines for the south, and the dashed lines for the north sample for each k -value. The values of k range from $0.20 h\text{Mpc}^{-1}$ at the top to $3.2 h\text{Mpc}^{-1}$ at the bottom with an increment of $\Delta \log_{10} k = 0.2$. The south and north samples agree quite well with the full survey indicating that cosmic variance is not a problem. The solid lines are the best fits obtained by applying equation (2) to the data of the whole survey. The power spectrum for the larger k -values decreases quite strongly with μ , more than a factor of 10 between $\mu = 0$ and $\mu = 1$. There is a small luminosity dependence. $P^S(k, \mu)$ increases for the bright samples by a factor $\simeq 2$ for all k . A similar dependence on luminosity for the 2PCF was found by Norberg et al. (2002a) (see also the real space spectrum below).

In Fig. (6) the real space power spectrum of the 2dFGRS $P(k)$ is displayed for the four different luminosity intervals (symbols). Again we can see that $P(k)$ for brighter samples

are higher. The error bars are derived from the mock samples described in the previous section. We prefer this error estimate to the bootstrap method which in general gives 50% smaller errors. The mock sample errors are just the standard deviations occurring, when the identical analysis is carried out for the 20 mock samples. These error bars adequately include the sample to sample variations (the cosmic variance), and they are not sensitive to the bias model used (JMB98). The figure shows that $P(k)$ is quite reliably determined for k between $0.1 h\text{Mpc}^{-1}$ and $4 h\text{Mpc}^{-1}$. Although $P(k) = P^S(k, \mu = 0)$ in principle, $P(k, \mu = 0)$ fluctuates around the true value of $P(k)$ in practice, because in a finite sized survey the number of Fourier modes is always limited. $P(k)$ is better determined, if $P^S(k, \mu)$ at different angles is combined with $P(k)$ being treated as a free parameter, as is done here. The spectrum is approximately a power law for the range of k considered here. It decays with k approximately as $k^{-1.5}$, with the slope of the brightest sample somewhat shallower. The smooth solid lines are the predictions of the halo model of Yang et al. which is implemented as described in section 4. The agreement with the data is satisfactory on large scales where $k < 0.5 h\text{Mpc}^{-1}$, not a surprising fact, since the halo model has been constructed such as to reproduce the luminosity-dependent clustering length of the 2dFGRS (i.e. linear to quasi-linear regimes). Nevertheless, we may note that for samples 5, 7, and 9 the halo model gives an indication of a change in slope of $P(k)$ at $k = 1 h\text{Mpc}^{-1}$. This can be understood as the transition between the scales where the pair counts are dominated by galaxy pairs in the same halo to the larger scales, where pairs of galaxies mostly are in separate halos. In the data such a change in slope is much less pronounced, but it is present for the brightest samples (see also Y04, Zehavi et al. 2003). The discrepancy between the model and the 2dFGRS data at small scales of $k \gtrsim 1 h\text{Mpc}^{-1}$ is very significant, at $\sim 3\sigma$ level for sample 9, at $\sim 10\sigma$ level for sample 7, and at $\sim 5\sigma$ level for sample 5. We also note that the clustering of the faint sample (sample 3) is higher than the halo model on all scales at $\sim 1.5\sigma$ level.

The PVD is measured simultaneously with $P(k)$, and the results are presented in Fig. (7). It seems that for the k -values used here, $\sigma_{12}(k)$ is a well-determined quantity. For the faintest sample, the PVD is persistently higher than that of the halo model (at $\sim 2\sigma$ level), indicating that the faint galaxies in the Universe may reside in more massive halos than the halo model predicts. This can also explain why the $P(k)$ of this sample is systematically higher than the halo model prediction. For sample 5, the difference in the PVD between the 2dFGRS and the halo model is only 50 to 100 km s^{-1} , consistent with the fact that their $P(k)$ are also close, though the agreement is not very good as the discrepancy between the model and the observation is significant at 2σ level. For the bright galaxies (sample 7 and sample 9), the halo model prediction rises quickly with k at $k > 1 h\text{Mpc}^{-1}$, as the galaxy pairs on these scales are mainly contributed by those from the same massive halos. This behavior was also seen in the power spectrum $P(k)$ at small scale where $P(k)$

rises quickly with k . Especially for sample 7, the observed PVD does not rise with k and is only around 500 km s^{-1} , which is expected if the galaxies are more distributed among isolated halos with the velocity dispersion of $200 \sim 300 \text{ km s}^{-1}$ (bright spirals). For sample 9, the PVD rises with k , but much slower than the halo model around 1 hMpc^{-1} , which also indicates that the brightest galaxies in the real Universe are distributed more in halos of different mass than the halo model predicts. The difference between the halo model and the observation is significant at $> 3\sigma$ level for the bright samples.

The luminosity dependence of the PVD is shown most clearly in Fig. (8), where we have plotted σ_{12} at $k = 1 \text{ hMpc}^{-1}$ for the 10 overlapping samples listed in table 1. The surprising result is a strong dependence on luminosity with the bright and the faint galaxies reaching high values of $\simeq 700 \text{ km s}^{-1}$, and with a well defined minimum of $\simeq 400 \text{ km s}^{-1}$ for the galaxies of sample 8. The bright and the faint galaxies apparently have high random motions, as expected for objects in a massive halo or in a cluster. The M^* like galaxies are rather moderate in their PVD, and probably reside in galaxy size halos. The thick solid line represents the prediction based on the halo model of Y04 (§4) that clearly does not match our observation of the PVD.

5.2. Implications for the halo model

The results of Y04 as well as of the current work show that the halo model adopted in this paper can reproduce the luminosity function very well, but cannot match the clustering data of galaxies perfectly. The model can quite successfully account for the luminosity dependence of clustering on large scales (i.e. the luminosity dependence of the clustering length), though it seems to underpredict for the faintest galaxies (Figure 6). Moreover, the clustering at small scales ($r < 2 \text{ h}^{-1}\text{Mpc}$ or $k > 0.5 \text{ hMpc}^{-1}$) predicted by the model is higher than the 2dFGRS data by a factor of 2 to 3. Also the PVD and the quadrupole-to-monopole ratio of the redshift space correlation function are higher in the model than the 2dFGRS data when the luminosity classification has not been applied. To solve these problems (or part of them), Y04 proposed several possible solutions, that is, to raise the mass-to-light ratio to $1000(M/L)_\odot$ for rich clusters in the B-band, to introduce a strong velocity bias $b_{\text{vel}} \equiv \sigma_{\text{gal}}/\sigma_{\text{dm}} = 0.6$ (where σ_{gal} and σ_{dm} are the velocity dispersions of galaxies and dark matter in halos), or to lower the clustering amplitude σ_8 to about 0.7. As Y04 realized, the first two solutions are not realistic, because the observed mass-to-light ratio is $(450 \pm 100)(M/L)_\odot$ (Fukugita et al. 1998) and $(363 \pm 65)(M/L)_\odot$ (Carlberg et al. 1997) for rich clusters in the B-band, and hydro/N-body simulations show that velocity bias is rather minor for rich galaxy systems (Yoshikawa, Jing, & Börner 2003; Berlind et al. 2003).

Therefore we only consider the last possibility to see if a low $\sigma_8 = 0.7$ can bring the halo model into agreement with our luminosity-dependent PVD result.

In our N-body data library, we have one simulation with $L = 100 h^{-1}\text{Mpc}$ and another with $L = 300 h^{-1}\text{Mpc}$ in a $\sigma_8 = 0.7$ LCDM model. The model and simulation parameters of these two simulations are the same as those of the simulations with the same boxsize L in §4, except for that the density parameter $\Omega_0 = 0.25$ is slightly lower for the new model. Xiaohu Yang has kindly provided us with the parameters of the halo model for this cosmological model. We find that the luminosity function of the 2dFGRS can be reproduced and the clustering is improved on small scales (but still higher for luminosity bins around M^*) in this model. Its PVD is shown in Fig.8 as a function of luminosity, which is considerably lower than the data of 2dFGRS. Compared with the low σ_8 model of Y04, our Ω_0 is slightly lower. Since the PVD is approximately proportional to $\sigma_8 \Omega_0^{0.6}$, we can boost the PVD by $(0.30/0.25)^{0.6}$ which is also shown in Fig.8. We can see that this PVD after correcting for the Ω_0 difference is still lower than our 2dFGRS data. More interestingly, this low σ_8 model also predicts a monotonically decreasing PVD with the decrease of the luminosity, implying that simply changing the value of σ_8 cannot overcome the difficulty of the halo model to explain the bimodal nature of the luminosity dependence of the PVD.

It should be possible to use the PVD to constrain the value of σ_8 if the shape of the PVD is reproduced in the halo model. Y04 argued for $\sigma_8 = 0.7$ from a comparison with the 2dFGRS PVD without a luminosity classification (Hawkins et al. 2003) (see also van den Bosch, Mo, & Yang 2003, for other independent arguments), but our comparison of the halo model with our 2dFGRS data seems to favor a higher σ_8 , since the PVD of the this low σ_8 model is lower than the observed data at all luminosities. Considering that most of the 2dFGRS galaxies are in the luminosity interval $-20.5 < M_b - 5 \log_{10} h < -18.5$, we would require $\sigma_8 \approx 0.82$ for the $\Omega_0 = 0.3$ according to the $\sigma_8 \Omega_0^{0.6}$ scaling if we want the halo model to match the observed PVD at $M_b - 5 \log_{10} h = -19.5$. This value of σ_8 is in good agreement with the recent determinations based on the WMAP and the SDSS galaxy-galaxy lensing data (Spergel et al. 2003; Seljak et al. 2004a). Although this is not a rigorous determination for σ_8 because we have not yet reproduced the shape of the luminosity dependence of PVD, our comparison indicates that the concordance model favored by the WMAP and SDSS data is consistent with our PVD data.

The PVD is an indicator of the depth of the local gravitational potential. Therefore we are inevitably led to the interesting conclusion that the bright and the faint galaxies move in the strongest gravitational field. A substantial fraction of them must be in clusters, while most galaxies around magnitude $M_b - 5 \log_{10} h = -20.5$, the M^* galaxies in the Schechter luminosity function, populate the field. We believe this result, that is, the shape of the PVD

luminosity dependence (not its absolute amplitude), constitutes a new challenge to the halo model of Yang et al.. The straightforward implication for the halo model is to increase the faint galaxy population in rich clusters. With the parameters of the Yang et al.’s halo model, the faint end slope α_{15} of their conditional luminosity function in rich clusters is one of the crucial quantities that determine the fraction of the faint galaxies in rich clusters. We expect that decreasing α_{15} (i.e. steeper faint end slope) can increase the fraction of faint galaxies in rich clusters. It is therefore worth investigating if a more negative α_{15} than the value -1.32 of the M1 model can save the halo model of Y03.

It is important to emphasize that the conditional luminosity function method proposed by Yang et al. is a highly valuable approach to infer the galaxy distribution within dark halos from a wide range of observations. The discrepancy between the M1 model and our PVD luminosity dependence (especially the bimodal shape of the PVD) does not necessarily mean that the halo model approach is wrong or useless. Instead it does mean that the luminosity dependence of the PVD provides an important test for galaxy formation models that is independent of the correlation functions. Because the PVD is more sensitive to the small number of galaxies in rich clusters than the correlation function (Mo, Jing, & Börner 1993; Mo, Jing, & Borner 1997), combining these two types of statistical quantities can put a more stringent constraint on the parametrization of the halo model.

The galaxy-galaxy lensing of the SDSS constrains strongly the fraction of faint galaxies in rich clusters (Sheldon et al. 2004; McKay et al. 2002). The rapid decrease of the lensing signal with the luminosity of the lensing galaxies indicates that the average matter density around galaxies decreases with the decrease of galaxy luminosity (Tasitsiomi, et al. 2004; Seljak et al. 2004b). However, the galaxy-galaxy lensing observation may not be inconsistent with our PVD observation that quite a fraction of faint galaxies are in rich clusters. The main reason is that these two quantities as well as the two-point correlation function depend on the halo occupation number of galaxies differently. In other word, the faint population in rich clusters has a different weight on these different quantities. Because of its pair-square weighting nature, the PVD statistic is mostly sensitive to those faint galaxies in rich clusters (Mo, Jing, & Borner 1997). Because the mean lensing signal (Sheldon et al. 2004) is galaxy number weighted, the lensing statistic may be much less sensitive to the faint population in rich clusters than the PVD. Figure 6 also shows that the two-point correlation predicted by the current halo model (M1 model) is about 50 percent lower than the observed value for faint galaxies, indicating there is room for increasing faint galaxies in rich clusters. It would certainly be very interesting to examine quantitatively if such a halo model can be constructed to consistently interpret all these three quantities. Because these quantities depend on the halo occupation number in different manners, we expect that they will play important but complementary roles in constraining the halo occupation of galaxies.

6. Conclusions

The analysis of the velocity fields of the galaxies in the 2dFGRS (C01) has led to a surprising discovery: The random velocities of the faint galaxies are very high, around 700 km s^{-1} , reaching similar values as the bright galaxies. At intermediate luminosities the velocities exhibit a well defined steep minimum near 400 km s^{-1} .

It seems that the galaxies in different luminosity intervals appear as different populations in their own right, defined by objective statistics. A look at Fig. (8) shows convincingly that this is actually the case. For this figure we have sorted the galaxies in 10 luminosity bins, each one magnitude wide, from magnitude -16.5 to -22 and plotted the value of σ_{12} at a wave number of $k \simeq 1 \text{ hMpc}^{-1}$. Such a finely resolved binning of galaxies in samples of different luminosities is possible for the 2dFGRS redshift survey, because it is big enough to contain sufficiently many galaxies in each luminosity class. In each bin the PVD is a well defined quantity which can be measured reliably (the very luminous galaxies have large error bars, because there are very few pairs of such objects at those scales).

The PVD is an indicator of the depth of the local gravitational potential. Therefore we find the interesting result that the bright and the faint galaxies move in the strongest gravitational field. A substantial fraction of them must be in clusters, while most galaxies around magnitude $M_b - 5 \log_{10} h = -20.5$, the M^* galaxies in the Schechter luminosity function, populate the field.

The bimodal nature of the correlation between PVD and luminosity may be used as a stringent test of galaxy formation models. We have investigated the halo occupation model (Y03) which has been optimally fitted to reproduce the luminosity function, and the two-point correlation function of the 2dFGRS. If we adapt this model to the PVD value of the M^* galaxies, we see that it cannot give the high values found for the fainter galaxies. The PVD values of the model actually run opposite to the data and the model assigns smaller values to the fainter galaxies. This indicates that the assignment of galaxies to the dark matter halos must be done in a more intricate way as up to now. In Table 2 we have listed the PVD values for the different luminosity bins. These must be reproduced by an acceptable model for galaxy formation. The number of faint galaxies in clusters must be increased substantially to at least recover the high PVD found for them. One possible solution for the halo model is to raise the faint end slope of the conditional luminosity function in rich clusters. Also, the low value of 400 km s^{-1} found for the galaxies with magnitude -20.5 must mean that these galaxies reside in dark matter halos of galactic size,

Another way, widely used, to connect dark matter to galaxies is the semi-analytic modeling (e.g., Kauffmann et al. 1999; Cole et al. 2000; Benson et al. 2000; Somerville & Primack

1999; Diaferio et al. 1999; Springel et al. 2001), where the dark matter distributions obtained from N-body simulations are supplemented with some of the physical processes important in galaxy formation using semi-analytic techniques. A test of the PVD vs luminosity for this type of models will be the aim of a subsequent paper.

We have shown here in addition that our novel method of deriving the real space power spectrum and the PVD from the redshift space power spectrum allows to determine these quantities precisely and reliably from the 2dFGRS. The size of the 2dFGRS permits an investigation of the luminosity dependence of these quantities. New constraints on galaxy formation models can be derived from that. We have shown that the luminosity dependence of the clustering can be reproduced by an adequately chosen halo occupation model. This model fails, however, to reproduce the luminosity dependence of the PVD.

We are grateful to Houjun Mo for a very stimulating and helpful discussion on the halo model, Uros Seljak for his helpful comment on the galaxy-galaxy lensing observation, and Xiaohu Yang for providing the halo model parameters of the low σ_8 model and for some instructions of implementing the halo model in N-body simulations, and the anonymous referee for helpful comments that improve our presentation. JYP would like to thank the Max-Planck Institute für Astrophysik for its warm hospitality during the time when this work was completed. GB wants to thank the Shanghai Astronomical Observatory for friendly infrastructure provided during his stay in Shanghai. The work is supported in part by NKBRSP (G19990754), by NSFC (Nos.10125314, 10373012), and by the CAS-MPG exchange program.

REFERENCES

Bardeen J. M., Bond J. R., Kaiser N., Szalay A. S. 1986, ApJ, 304, 15
Benson A. J., Baugh C. M., Cole S., Frenk C. S., Lacey C. G., 2000, MNRAS, 316, 107
Berlind, A. A. & Weinberg, D. H. 2002, ApJ, 575, 587
Berlind A.A., et. al., 2003, ApJ, 593, 1
Carlberg R.G., Morris S.L., Yee H.K.C., Ellingson E., 1997, ApJ, 479, L19
Cole, S., Fisher, K. B., & Weinberg, D. H. 1995, MNRAS, 275, 515
Cole, S., Lacey, C. G., Baugh, C. M., & Frenk, C. S. 2000, MNRAS, 319, 168

Colless, M. et al. 2001, MNRAS, 328, 1039

Colless, M. et al. 2003, astro-ph/0306581

Davis M., Peebles P.J.E., 1983, ApJ, 267, 465

Diaferio, A., Kauffmann, G., Colberg, J. M., & White, S. D. M. 1999, MNRAS, 307, 537

Fisher, K. B., Davis, M., Strauss, M. A., Yahil, A., & Huchra, J. P. 1994b, MNRAS, 267, 927

Fisher, K. B., Davis, M., Strauss, M. A., Yahil, A., & Huchra, J. 1994a, MNRAS, 266, 50

Fukugita M., Hogan C.J., Peebles P.J.E., 1998, ApJ, 503, 518

Hamilton, A. J. S. & Tegmark, M. 2002, MNRAS, 330, 506

Hawkins et al. 2003, MNRAS, 346, 78

Jing, Y. P. 2002, MNRAS, 335, L89

Jing, Y. P. & Börner, G. 1998, ApJ, 503, 37

Jing Y.P., Börner G., 2001, ApJ, 547, 545

Jing, Y. P. & Börner, G. 2001, MNRAS, 325, 1389

Jing, Y. P. & Börner, G. 2004, ApJ, 607, 140

Jing, Y. P., Börner, G., & Suto, Y. 2002, ApJ, 564, 15

Jing, Y. P., Mo, H. J., & Börner, G. 1998, ApJ, 494, 1

Jing, Y. P. & Suto, Y. 2002, ApJ, 574, 538

Juszkiewicz R., Fisher K.B., Szapudi I. 1998, ApJ, 504, L1

Kaiser, N. 1987, MNRAS, 227, 1

Kang, X., Jing, Y. P., Mo, H. J., & Börner, G. 2002, MNRAS, 336, 892

Kauffmann, G., Colberg, J. M., Diaferio, A., & White, S. D. M. 1999, MNRAS, 303, 188

Landy, S. D., Szalay, A. S., & Broadhurst, T. J. 1998, ApJ, 494, L133

Marzke, R. O., Geller, M. J., da Costa, L. N., & Huchra, J. P. 1995, AJ, 110, 477

McKay, T. A., et al. 2002, preprint (astro-ph/0108013)

Mo H.J., Jing Y.P., Börner G., 1993, MNRAS, 264, 825

Mo, H. J., Jing, Y. P., & Borner, G. 1997, MNRAS, 286, 979

Norberg, P. et al. 2001, MNRAS, 328, 64

Norberg, P. et al. 2002a, MNRAS, 332, 827

Norberg, P. et al. 2002b, MNRAS, 336, 907

Peacock, J. A. & Dodds, S. J. 1994, MNRAS, 267, 1020

Peacock, J. A., et al. 2001, Nature, 410, 169

Pearce, F. R., Jenkins, A., Frenk, C. S., White, S. D. M., Thomas, P. A., Couchman, H. M. P., Peacock, J. A., & Efstatthiou, G. 2001, MNRAS, 326, 649

Peebles P.J.E., 1976, Ap&SS45, 3

Peebles P.J.E., 1980, The Large-Scale Structure of the Universe, Princeton University Press, Princeton

Scoccimarro, R. 2004, ArXiv Astrophysics e-prints, astro-ph/0407214

Sheth, R. K., Hui, L., Diaferio, A., & Scoccimarro, R. 2001, MNRAS, 325, 1288

Seljak, U., et al. 2004a, ArXiv Astrophysics e-prints, astro-ph/0407372

Seljak, U., et al. 2004b, ArXiv Astrophysics e-prints, astro-ph/0406594

Sheldon, E. S., et al. 2004, AJ, 127, 2544

Somerville, R. S., Davis, M., & Primack, J. R. 1997, ApJ, 479, 616

Somerville, R. S. & Primack, J. R. 1999, MNRAS, 310, 1087

Spergel D.N., et al., 2003, ApJS, 148, 175

Springel V., White S.D.M., Tormen G., Kauffmann G., 2001, MNRAS, 328, 726

Tasitsiomi, A., Kravtsov, A. V., Wechsler, R. H., & Primack, J. R. 2004, astro-ph/0404168

van den Bosch, F. C., Mo, H. J., & Yang, X. 2003, MNRAS, 345, 923

Weinberg, D. H., Davé, R., Katz, N., & Hernquist, L. 2004, ApJ, 601, 1

Yang, X., Mo, H. J., Jing, Y. P., van den Bosch, F. C., & Chu, Y. 2004, MNRAS, 350, 1153

Yang, X., Mo, H. J., & van den Bosch, F. C. 2003, MNRAS, 339, 1057

Yan, R., Madgwick, D. S., & White, M. 2003, ApJ, 598, 848

Yoshikawa K., Jing Y.P., Börner G. 2003, ApJ, 590, 654

Zehavi, I. et al. 2002, ApJ, 571, 172

Zehavi, I. et al. 2003, astro-ph/0301280

Table 1: Samples selected according to luminosity

Sample	$M_b - 5 \log_{10} h$	South (no. of galaxies)	North (no. of galaxies)	Total (no. of galaxies)
1	$-16.5 > M_b - 5 \log_{10} h \geq -17.5$	5218	3587	8805
2	$-17.0 > M_b - 5 \log_{10} h \geq -18.0$	9314	6078	15392
3	$-17.5 > M_b - 5 \log_{10} h \geq -18.5$	14593	11097	25690
4	$-18.0 > M_b - 5 \log_{10} h \geq -19.0$	23703	18670	42373
5	$-18.5 > M_b - 5 \log_{10} h \geq -19.5$	34481	25683	60164
6	$-19.0 > M_b - 5 \log_{10} h \geq -20.0$	40995	29241	70236
7	$-19.5 > M_b - 5 \log_{10} h \geq -20.5$	40182	27223	67405
8	$-20.0 > M_b - 5 \log_{10} h \geq -21.0$	30934	19204	50138
9	$-20.5 > M_b - 5 \log_{10} h \geq -21.5$	15388	8848	24236
10	$-21.0 > M_b - 5 \log_{10} h \geq -22.0$	3739	2162	5901

Table 2: The results of the PVD at $k = 1 \text{ hMpc}^{-1}$ of the luminosity subsamples

Sample	Median Mag. $M_b - 5 \log_{10} h$	$\sigma_v[\beta = 0.45]^a$ (km s^{-1})	$\sigma_v[\beta(L)]^b$ (km s^{-1})
1	-17.15	698 ± 103	717 ± 102
2	-17.62	642 ± 73	659 ± 72
3	-18.12	723 ± 88	737 ± 87
4	-18.61	686 ± 42	697 ± 42
5	-19.06	609 ± 23	616 ± 23
6	-19.51	498 ± 24	500 ± 24
7	-19.96	468 ± 21	463 ± 21
8	-20.39	424 ± 17	412 ± 17
9	-20.76	599 ± 44	580 ± 44
10	-21.18	979 ± 303	945 ± 296

^aThe PVD determined with $\beta = 0.45$.

^bThe PVD determined with the luminosity dependence of β taken into account.

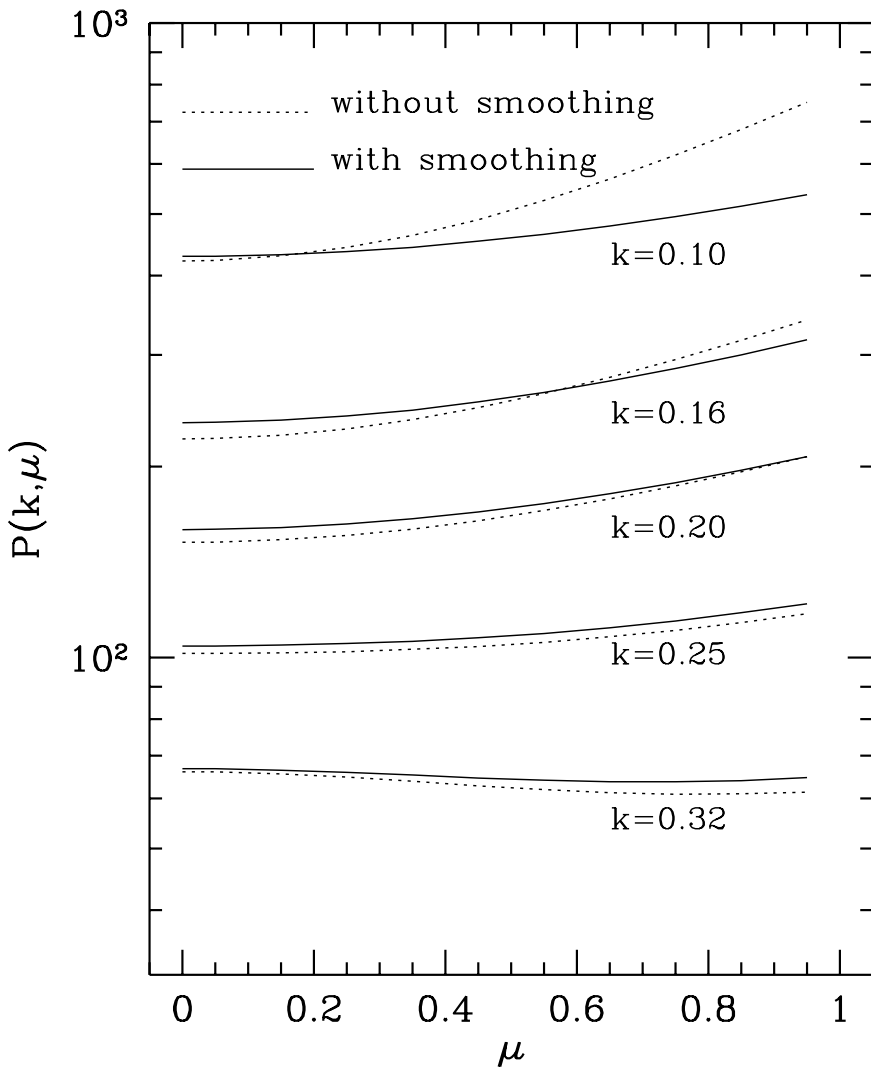


Fig. 1.— Illustration of the smoothing effect on the determination of the redshift space power spectrum $P(k, \mu)$ when the redshift space two-point correlation function $\xi(r_p, \pi)$ is weighted by a Gaussian function of width $R = 20 h^{-1} \text{Mpc}$. The solid lines, computed with Eq.(10), are the $P(k, \mu)$ with the smoothing effect, compared to the dotted lines for $P(k, \mu)$ without the smoothing effect. In this plot, we use the linear CDM power spectrum of $\Gamma = 0.2$, $\beta = 0.45$ and $\sigma_v = 500 \text{ km s}^{-1}$ as input. k is in units of $h\text{Mpc}^{-1}$

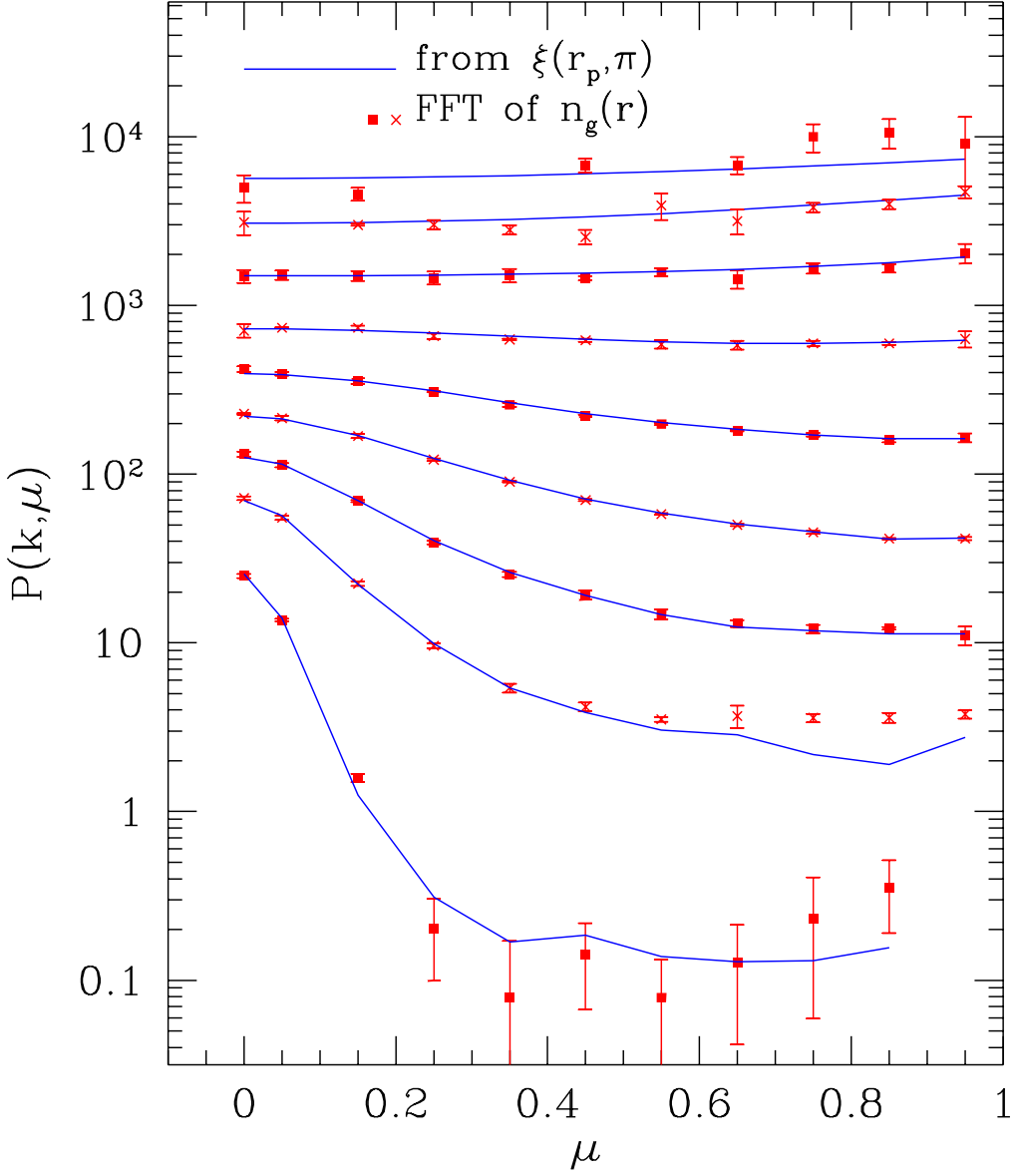


Fig. 2.— The simulation test of the statistical method used in this paper that measures $P(k, \mu)$ from $\xi(r_p, \pi)$. The solid lines are the measurement of $P(k, \mu)$ for a simulation sample of galaxies with $-19.5 < M_b - 5 \log_{10} h < -18.5$ based on the Gaussian weighted $\xi(r_p, \pi)$ measurement, compared with the direct measurement of $P(k, \mu)$ based on the Fourier transformation of the galaxy density field in redshift space (the symbols). From top to bottom, the wavelength k is $0.10, 0.16, 0.25, 0.40, 0.63, 1.0, 1.6, 2.5$, and $5.0 \text{ } h\text{Mpc}^{-1}$ respectively. The galaxies are produced with the halo model, and the simulations have a boxsize $L = 300 \text{ } h^{-1}\text{Mpc}$.

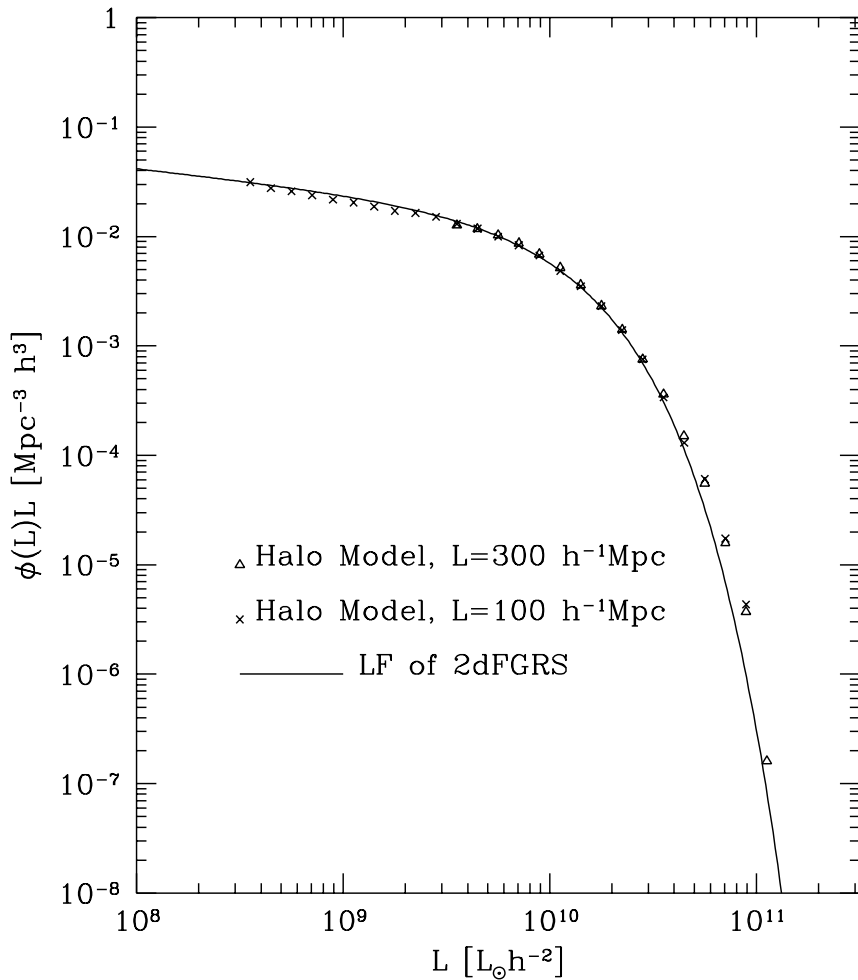


Fig. 3.— The luminosity function of galaxies generated with the halo model, compared with the observation of 2dFGRS. To the resolution limit $M_b - 5 \log_{10} h = -18.5$ for the simulation of $L = 300 h^{-1} \text{Mpc}$ and $M_b - 5 \log_{10} h = -16.5$ for the simulation of $L = 100 h^{-1} \text{Mpc}$, the luminosity functions of the mock galaxies agree well with the observed one, and agree with each other in the two simulations.

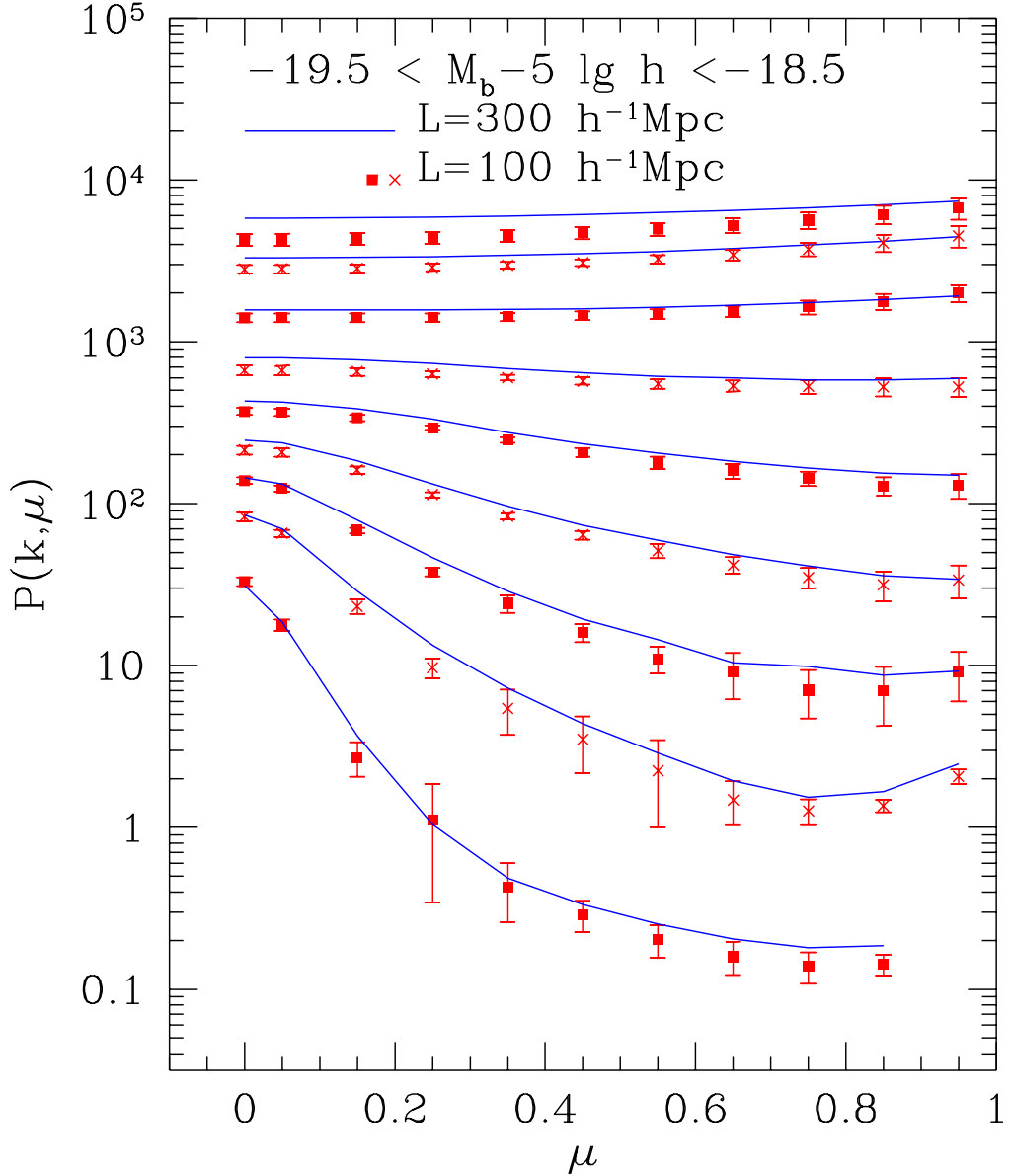


Fig. 4.— The resolution effect on the predicted $P(k, \mu)$ in simulations of different boxsizes. Galaxies of $-19.5 < M_b - 5 \log_{10} h < -18.5$ are analyzed. The results based on the 2dFGRS mock samples generated with $L = 100 h^{-1}\text{Mpc}$ simulations are plotted in symbols and those with $L = 300 h^{-1}\text{Mpc}$ simulations are plotted in connected lines. From top to bottom, the wavelength k is $0.10, 0.16, 0.25, 0.40, 0.63, 1.0, 1.6, 2.5$, and $5.0 h\text{Mpc}^{-1}$ respectively.

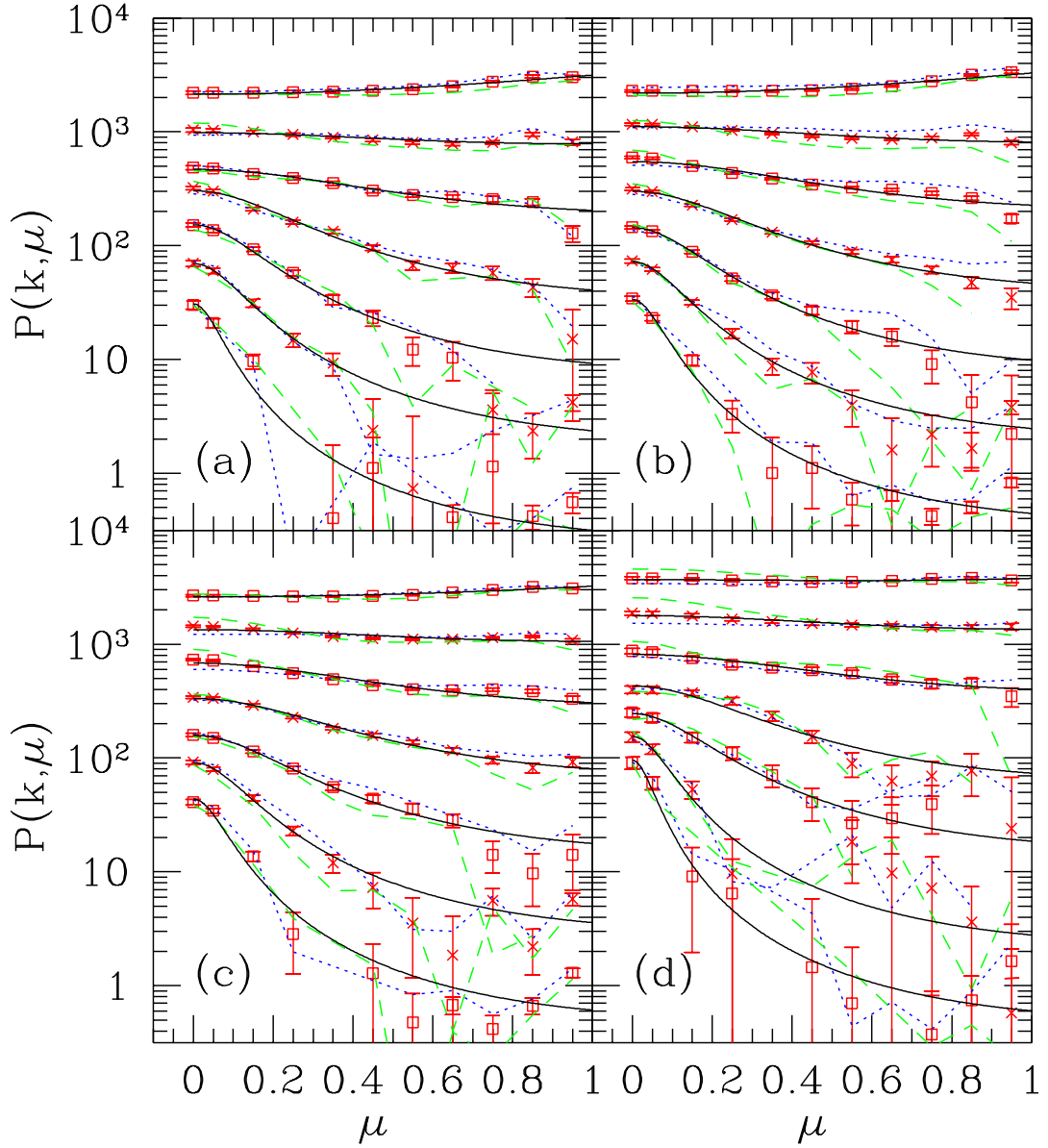


Fig. 5.— The redshift space power spectrum $P(k, \mu)$ measured in 2dFGRS. The symbols are for the whole survey, the dotted lines for the south subsample, and the dashed lines for the north subsample. The errors are plotted only for the whole survey that is estimated with the bootstrap method. The smooth solid lines are the best fits of Eq.(2) to data of the whole sample. (a) for $-18.5 < M_b - 5 \log_{10} h < -17.5$; (b) for $-19.5 < M_b - 5 \log_{10} h < -18.5$; (c) for $-20.5 < M_b - 5 \log_{10} h < -19.5$; (d) for $-21.5 < M_b - 5 \log_{10} h < -20.5$. In each panel from top to bottom, the wavelength k is $0.2, 0.32, 0.50, 0.79, 1.26, 2.0$, and 3.2 hMpc^{-1} respectively.

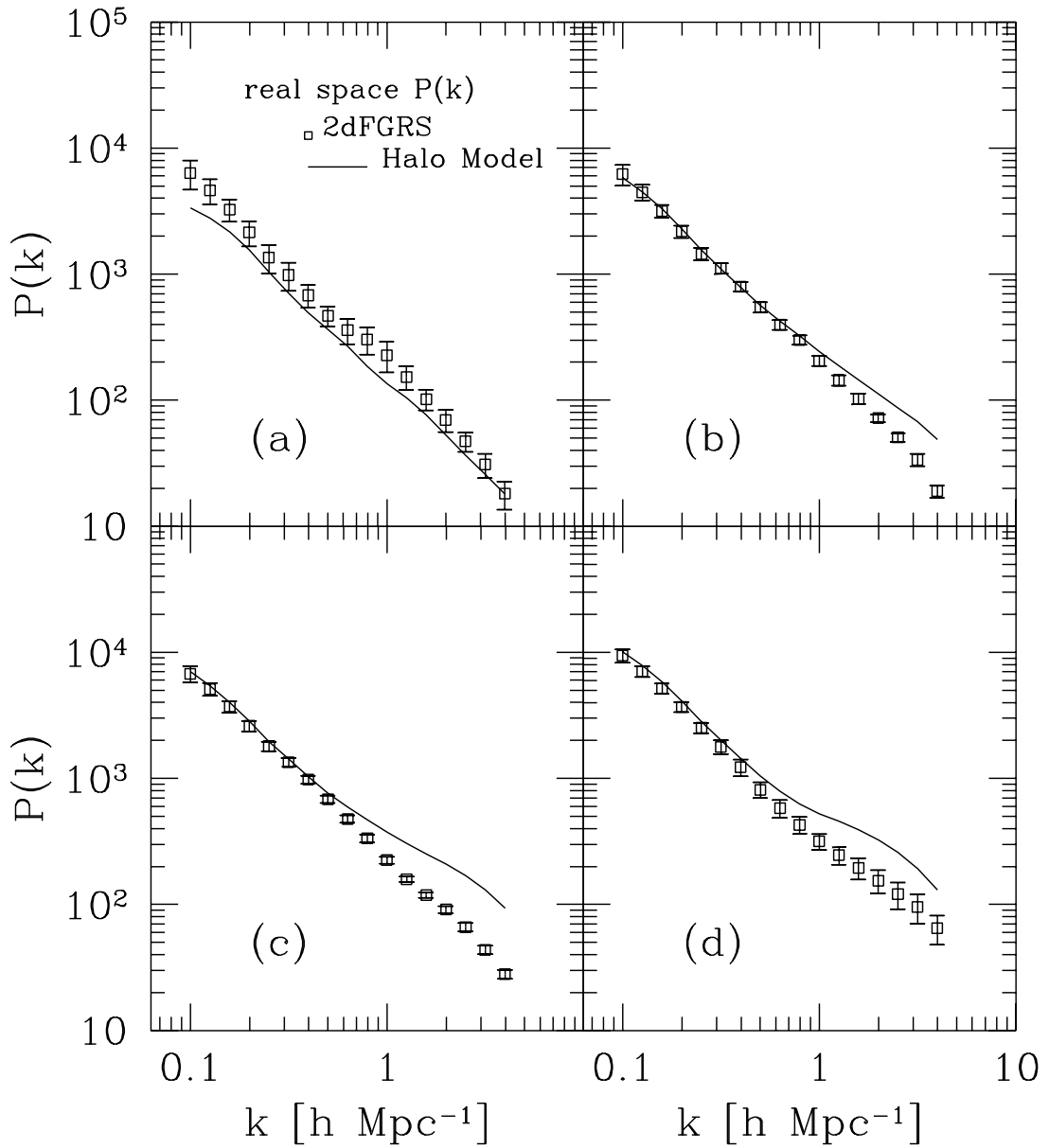


Fig. 6.— The real space power spectrum $P(k)$ measured in the 2dFGRS (symbols): a) for $-18.5 < M_b - 5 \log_{10} h < -17.5$, b) for $-19.5 < M_b - 5 \log_{10} h < -18.5$, c) for $-20.5 < M_b - 5 \log_{10} h < -19.5$, and d) for $-21.5 < M_b - 5 \log_{10} h < -20.5$. The error bars of the observed results are given by the mock samples, as described in the text. The smooth lines are the predictions based on the halo model.

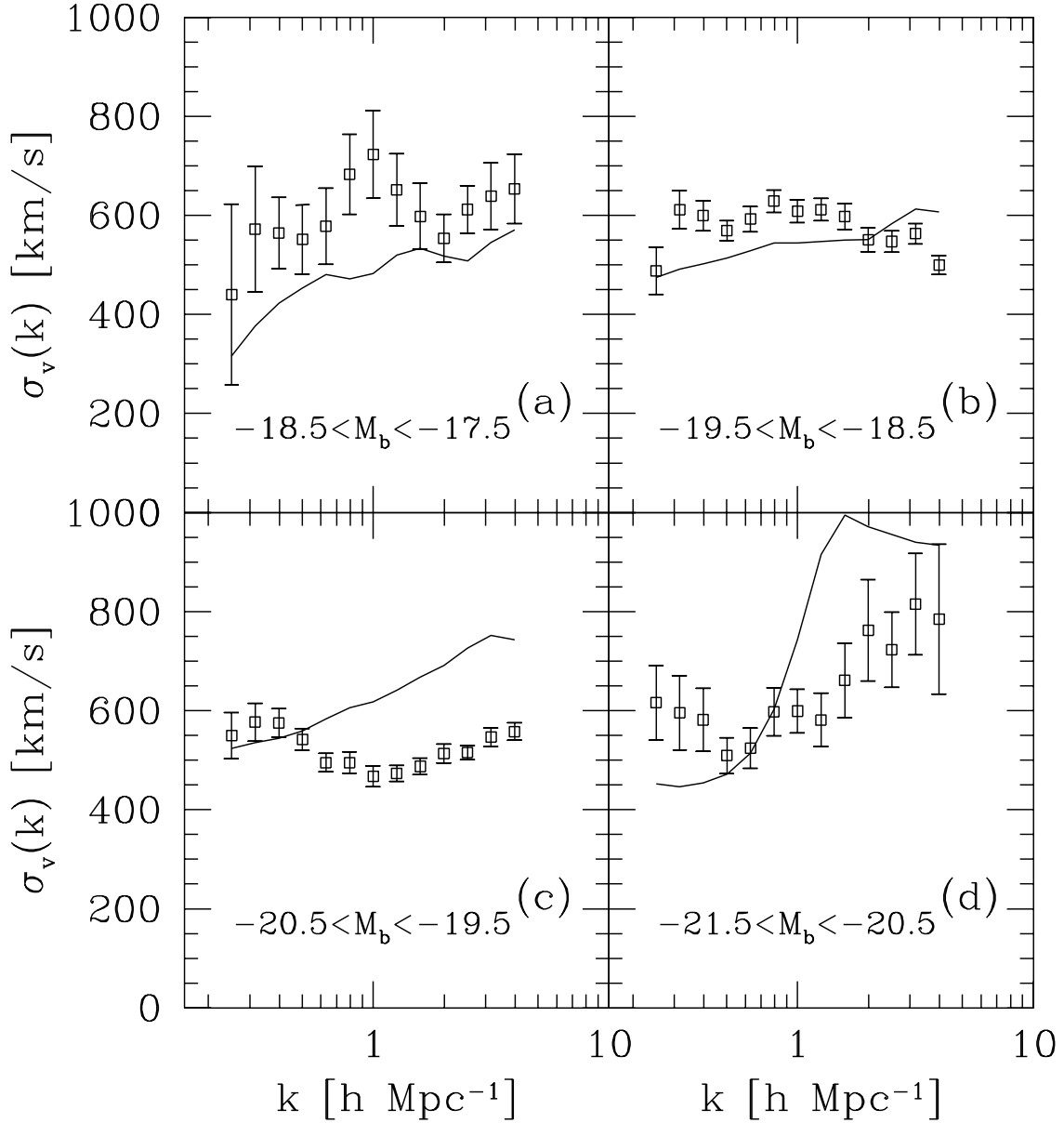


Fig. 7.— The PVD of galaxies measured in the 2dFGRS (symbols), compared with the predictions based on the halo model (solid lines). The error bars of the observed results are given by the mock samples, as described in the text.

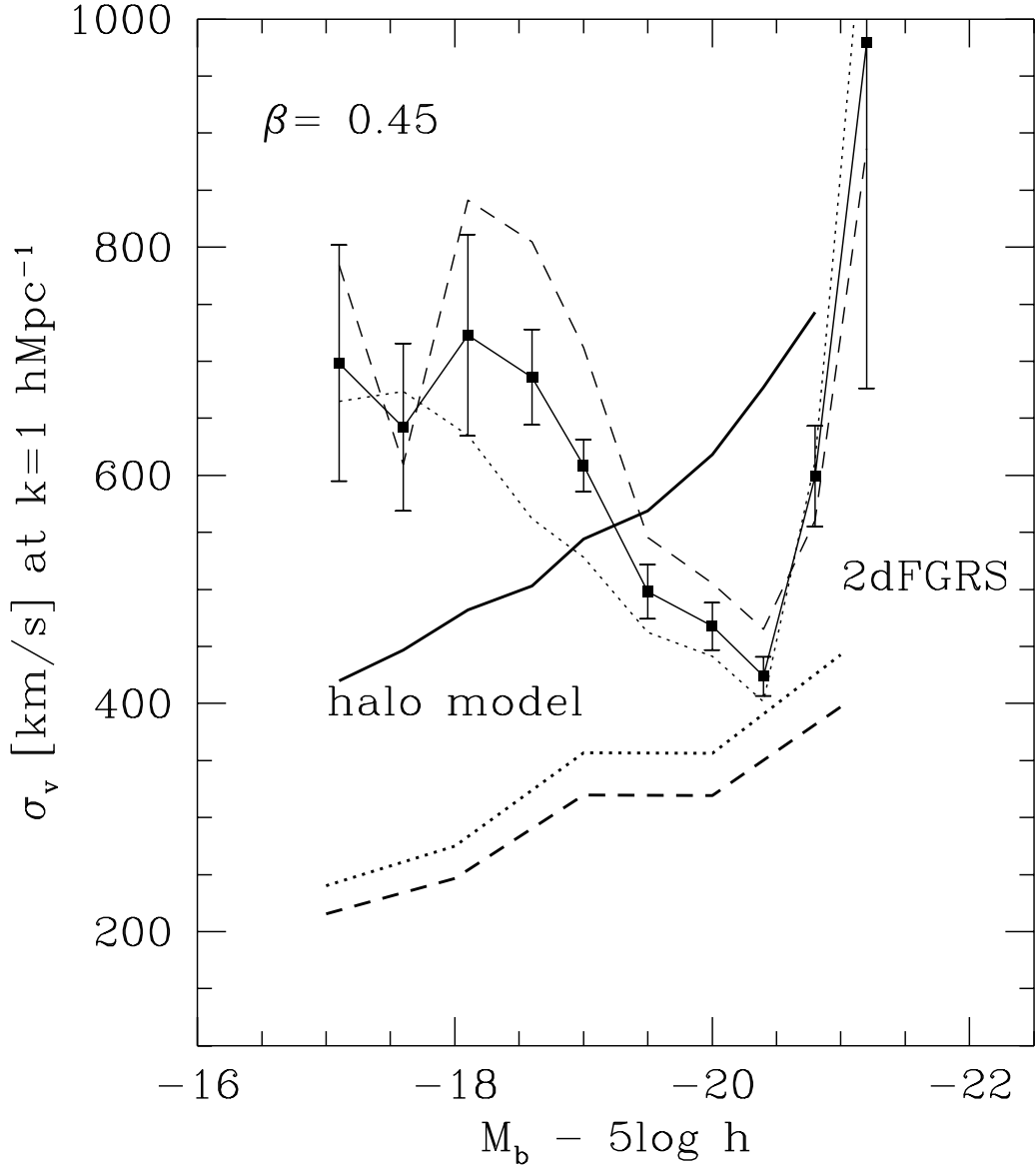


Fig. 8.— The PVD measured at $k = 1 \text{ hMpc}^{-1}$ in the 2dFGRS (symbols for the whole sample, dotted line for the south, and dashed line for the north), compared with the predictions based on the halo model. The thick solid line is for the nominal model of $\sigma_8 = 0.9$, the thick dashed one is for the model of $\sigma_8 = 0.7$, and the thick dotted one is for the model of $\sigma_8 = 0.7$ but with $\Omega_0 = 0.3$. The error bars of the observed results are given by the mock samples, as described in the text.

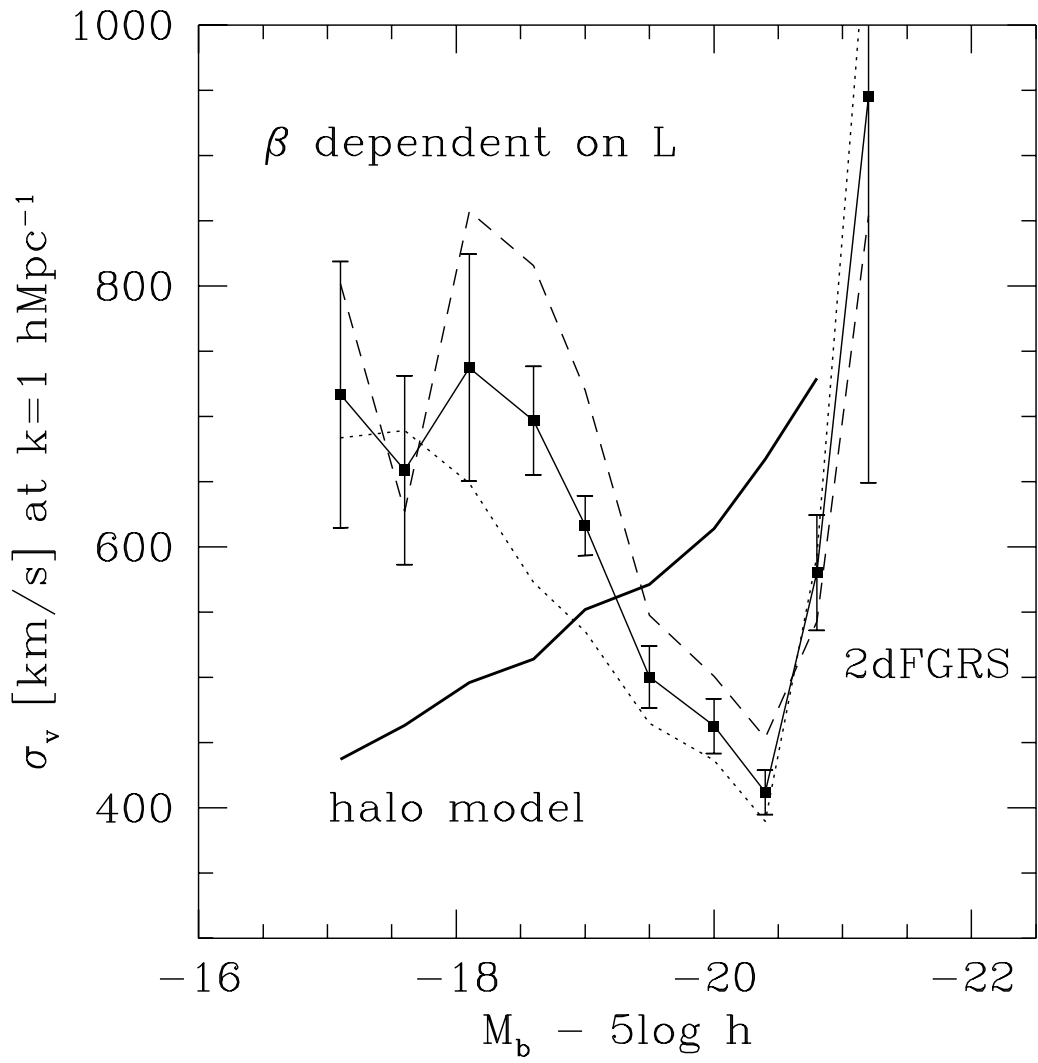


Fig. 9.— The PVD measured at $k = 1 h\text{Mpc}^{-1}$ in the 2dFGRS. Symbols have the same meaning as in Fig. (8). Here the parameter β varies with luminosity as in Norberg et al. (2002a).